URSI GASS 2020, Rome, Italy, 29 August - 5 September 2020

Using NUFFTs for interpolations of fast backprojection algorithms

Amedeo Capozzoli, Claudio Curcio, Angelo Liseno
(1) Universitá di Napoli Federico II, Dipartimento di Ingegneria Elettrica e delle Tecnologie dell'Informazione,
via Claudio 21, I 80125 Napoli (Italy); e-mail: a.capozzoli@unina.it.

Abstract

We deal with the interpolation problem of the Back-Projection (BP) and Fast Back-Projection (FBP) algorithms used in Synthetic Aperture Radar (SAR).
The needed 1D and 2D interpolations must be properly performed to mitigate the effect of the truncation error and achieve accurate results and can be effectively performed by adopting NUFFT routines.

1 Introduction

The back-projection (BP) algorithm is often used in Synthetic Aperture Radar (SAR) when accuracy is required and when curved trajectories must be dealt with. However, BP is computationally demanding, with a complexity equal to $P(N)+\mathcal{O}(N^2logN)$ for an $N\times N$ image: $\mathcal{O}(N^2logN)$ accounts for the FFT step and $P(N)$ is a polynomial associated to the interpolation between uniform and non-uniform grids [1,2]. Typically, $P(N)$ is $\mathcal{O}(N^4)$ or $\mathcal{O}(N^3)$ [3,4].
Fast BP (FBP) [5] reduces the complexity of BP to $\mathcal{O}(N^{5/2})$. However, FBP shows losses of accuracy due to the need of applying interpolations a large number of times. Interpolation errors can accumulate, especially at the edges of the interpolation domains.
BP has been recently improved using 1D Non-Uniform FFTs (NUFFTs) [1, 2], so achieving a $\mathcal{O}(N^2logN)$ complexity and a very convenient trade-off between complexity and accuracy. Furthermore, in FBP, the aperture partitionings lead to the calculation of partial images which can be performed as in the BP. Finally, such partial images require 2D interpolation stages [6] to combine them into common computational grids. So, effective interpolation is a fundamental step for either BP or FBP.
The aim of this paper is twofold: 1) underline that the computation of the partial images in FBP can be performed by using 1D NUFFT routines as in BP; 2) show that the 2D interpolations requested by FBP can be accurately worked out by 2D NUFFTs.

2 NUFFT-based BP

The geometry is illustrated in Fig. 1.
Here, for the sake of simplicity, a rectilinear trajectory is assumed although curved paths represent the case of interest in practice. Nevertheless, the approach can be applied to arbitrary flight trajectories as well.
We use the following symbols: t - slow time; c - light speed; $\underline{r}_a(t)=(x_a(t),y_a(t),z_a(t))$ - flight trajectory; (x,y) - ground coordinates.
BP approximates the ground reflectivity $\gamma(x,y)$ as [1,2]

$$h(x,y)=\sum_n \int S(t_n,f)e^{j2\pi f\frac{2\Delta R(x,y,t_n)}{c}}df \qquad (1)$$

where t_n is the slow-time instant at which the n-th pulse illuminating the scene is sent, $S(t_n,f)$ is the n-th signal after range compression of the raw data, f is the frequency, $\Delta R(x,y,t_n)=R(x,y,t_n)-R_a(t_n)$, $R_a(t_n)=||\underline{r}_a(t_n)||$, $R(x,y,t_n)=||\underline{r}-\underline{r}_a(t_n)||$ and $\underline{r}=(x,y,0)$.
Let us suppose the image grid to be the Cartesian grid (x_i,y_k). Eq. (1) then becomes

$$h(x_i,y_k)=\sum_q S(t_n,f_q)\,e^{j2\pi f_q\frac{2\Delta R((x_i,y_k),t_n)}{c}}\Delta f. \qquad (2)$$

Expression (2) can be efficiently and effectively computed by using a 1D NUFFT of Non-Equispaced Results (NER) type [7,8], being the input sampling f_q regular, but the output sampling defined by $2\Delta R((x_i,y_k),t_n)/c$ irregular.

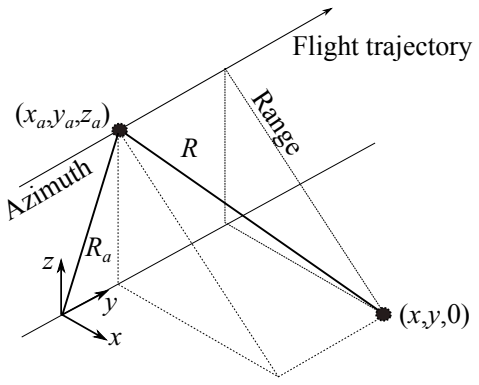

Figure 1. The considered SAR geometry.

3 The FBP and the 2D NUFFT-based interpolations

FBP divides the aperture into smaller sub-apertures of length l (Fig. 2), each associated to a partial image $h_m(x,y)$ [5]. The final image is obtained as a coherent superposition of the $h_m(x,y)$'s, namely

$$h(x,y) = \sum_m h_m(x,y) = \sum_m \sum_n s\left(t_{mn}, \frac{2\Delta R((x,y),t_{mn})}{c}\right), \tag{3}$$

where t_{mn} is the generic sampling point of the m-th sub-aperture. Each $h_m(x,y)$ can be efficiently and effectively computed according to the above BP scheme.
Letting $\bar{t}_m$ be the slow time at the center of the m-th sub-aperture, the generic sampling point t_{mn} of the m-th sub-aperture can be rewritten by aid of the center offsets ξ_n as $t_{mn} = \xi_n + \bar{t}_m$.
FBP is based on the fact that the partial images can be computed in a fast way with a controllable degree of approximation. Indeed, let us introduce a polar coordinate system $(\rho_m(x,y), \alpha_m(x,y))$ for the m-th sub-aperture defined as (Fig. 2)

$$\begin{cases} \rho_m = |\underline{r} - \underline{r}_a(\bar{t}_m)| \\ \cos\alpha_m = \frac{(\underline{r}-\underline{r}_a(\bar{t}_m))\cdot(\underline{r}_a(\xi_n+\bar{t}_m)-\underline{r}_a(\bar{t}_m))}{\rho_m \xi_n} \end{cases}, \tag{4}$$

with $\underline{r} = (x,y,0)$. Since

$$\Delta R(x,y,\xi_n+\bar{t}_m) = \sqrt{\rho_m^2(x,y) + \xi_n^2 - 2\rho_m(x,y)\xi_n \cos\alpha_m(x,y)} - R_a(\xi_n+\bar{t}_m), \tag{5}$$

the partial images can be regarded as function of the polar coordinate systems, i.e., $h_m = h_m(\rho_m, \alpha_m)$. A uniform polar grid $(\rho_{mh}, \alpha_{mr}) = (h\Delta\rho_m, r\Delta\alpha_m)$ can be chosen according to the following steps [5]

$$\Delta\rho_m \le \frac{c}{2BW}, \quad \Delta\alpha_m \le \frac{c}{2f_b l}, \tag{6}$$

where BW and f_b are the bandwidth and the maximum frequency of the illuminating pulse, respectively. The angular resolution is inversely proportional to the sub-aperture length which means that keeping l small enables weakening the angular sampling requirements.
FBP requires not only the computation of the partial images $h_m(h\Delta\rho_m, r\Delta\alpha_m)$ on the uniform polar grid $(h\Delta\rho_m, r\Delta\alpha_m)$, but also a 2D Polar-to-Cartesian interpolation onto the common Cartesian grid $(i\Delta x, k\Delta y)$ avoiding the error accumulation [5]. The mapping between the generic polar grid and the final Cartesian grid is illustrated in Fig. 3. Note that the uniform Cartesian grid $(i\Delta x, k\Delta y)$ appears as a non-uniform grid in polar coordinates. Here, we exploit the a priori information on the bandlimitedness of the relevant functions to calculate and interpolate in one shot using a 2D NER-NUFFT based algorithm.
For the above 2D NUFFT-based interpolations, the error arising from the truncation due to the finiteness of the 2D spectral grid can be relevant. Accordingly, such interpolations must be properly improved by the use of a window function to control the truncation error and achieve accurate results. In this paper, the Approximate Prolate (AP) spheroidal wavefunction has been used [9, 10].

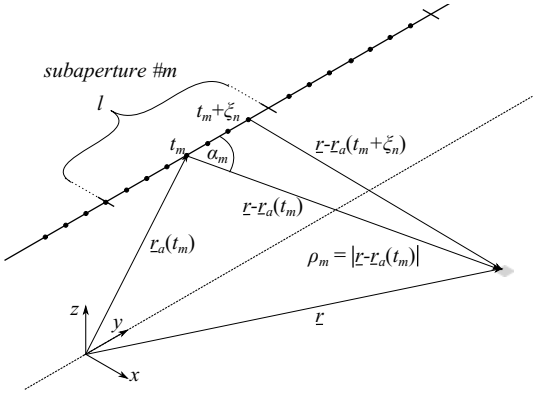

Figure 2. Relevant geometry for the FBP algorithm.

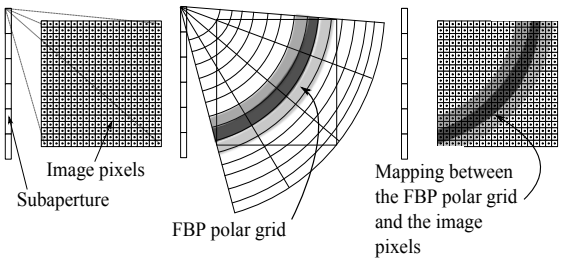

Figure 3. FBP: Mapping between the image pixels and the generic polar grid.

4 Numerical results

In this Section, we present an analysis to provide an estimate of the advantage of using the proposed approach for BP and FBP. The proposed interpolation is evaluated against other interpolators typically employed in this framework, namely, nearest-neighbor, linear, cubic and spline.
To assess the performance, we have considered a $10.24m \times 10.24m$ [11] scene with a solitary point scatterer at the scene center. Flight height and depression angle are $1km$ and $\pi/6$, respectively, while the number of pulses (azimuth positions) is 128. Center frequency and bandwidth are $10GHz$ and $600MHz$, respectively, for an overall number of 216 frequency points and 4096 FFT samples. The resolution has been $8cm \times 8cm$.

The reference image to compare with has been obtained by the BP approach in [1,2]. The approach in [1,2] is used as reference since, besides the approximation of the scattering model, the Green's function is exact and a minimum number of interpolations is employed.
For the reference BP case, 128 1D NUFFTs over 16384 samples are executed. Furthermore, for the FBP case, the data have been partitioned into 64 subapertures, with each subaperture involving a 2D NUFFT on 72×212 samples. In the FFBP case, a 6 levels hierarchy has been considered. A 37 samples Knab window has been considered for FBP.
In Figs. 3 and 4, the cuts along the x-axis of the normalized differences between the reconstructions achieved by the considered interpolators and the reference image is depicted for the BP and FBP cases, respectively. Furthermore, in Table 1, the (amplitude and phase) Root Mean Square (RMS) error between the reconstructions and the reference image are reported. The dramatic improvement of the considered interpolation scheme against the compared ones can be appreciated. It should be noticed that preserving the accuracy becomes more and more relevant when passing from BP to FBP since the number of requested interpolations increases.
It should be finally observed that the use of the NUFFT enables to modulate the trade-off between accuracy and computational complexity. For example, in some application cases, it could be unnecessary to reach the limits of double precision, as it occurs for Table 1, but reducing the accuracy to single precision could be a choice to speed up the processing.

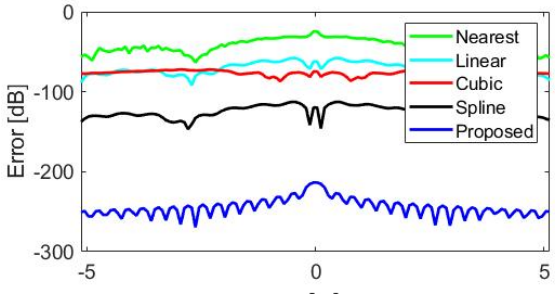

Figure 4. Error with the reference image: BP.

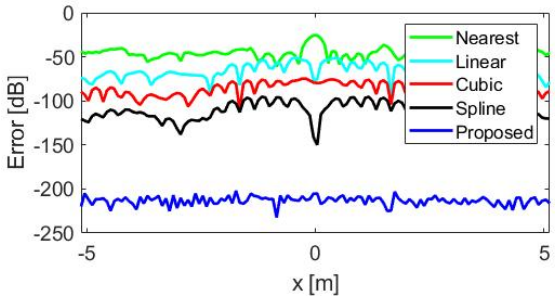

Figure 5. Error with the reference image: FBP.

Table 1. RMS values for the different interpolation algorithms

Algorithm	BP	FBP
Nearest	9.41%	16.3%
Linear	0.491%	2.28%
Cubic	0.263%	0.286%
Spline	0.00102%	0.0248%
Proposed	$2.35 \cdot 10^{-9}$%	$1.68 \cdot 10^{-8}$%

References

[1] A. Capozzoli, C. Curcio, A. di Vico, A. Liseno, "Nufft-& GPU-based fast imaging of vegetation", *IEICE Trans. Commun.*, vol. E94-B, n. 7, Jul. 2011, pp. 2092-2103.

[2] A. Capozzoli, C. Curcio, A. Liseno, "Fast GPU-based interpolation for SAR backprojection", *Progr. in Electromagn. Res.*, vol. 133, pp. 259-283, 2013.

[3] H. Choi, D.C. Munson, Jr., "Direct-Fourier reconstruction in tomography and synthetic aperture radar", *Int. J. Imaging Syst. Tech.*, vol. 9, n. 1, pp. 1-13, 1998.

[4] M.D. Desai, W.K. Jenkins, "Convolution backprojection image reconstruction for spotlight mode synthetic aperture radar", *IEEE Trans. Image Proc.*, vol. 1, n. 4, pp. 505-517, Oct. 1992.

[5] A.F. Yegulalp, "Fast backprojection algorithm for synthetic aperture radar", *Proc. of the IEEE Radar Conf.*, Waltham, MA, Apr. 20–22, 1999, pp. 60-65.

[6] P.O. Frölind, L.M.H. Ulander, "Evaluation of angular interpolation kernels in fast back-projection SAR processing", *IEE Proc.-Radar, Sonar, Navigat.*, vol. 153, n. 3, pp. 243 – 249, Jun. 2006.

[7] K. Fourmont, "Non-equispaced fast Fourier transforms with applications to tomography", *J. Fourier Anal. Appl.*, vol. 9, n. 5, pp. 431-450, Sept. 2003.

[8] A. Capozzoli, C. Curcio, A. Liseno, "Optimized Non-Uniform FFTs (NUFFTs) and their application to array factor computation", *IEEE Trans. Antennas Prop.*, vol. 67, n. 6, pp. 3924-3938, Jun. 2019.

[9] M. Migliaccio, *et al.*, "Knab sampling window for In-SAR data interpolation", *IEEE Geosci. Remote Sens. Lett.*, vol. 4, n. 3, pp. 397-400, Jul. 2007.

[10] J. Selva, "Interpolation of bounded bandlimited signals and applications", *IEEE Trans. Signal Proc.*, vol. 54, n. 11, pp. 4244-4260, Nov. 2006.

[11] U.K. Majumder, M.A. Temple, M.J. Minardi, E.G. Zelnio, "Point Spread Function characterization of a radially displaced scatterer using circular synthetic aperture radar", *Proc. of the IEEE Radar Conf.*, Boston, MA, Apr. 17-20, 2007, pp. 729-733.